

CHAPTER 5

LAYERED DOUBLE HYDROXIDE (LDHs) DERIVED MIXED OXIDES FOR SOLVENT FREE NITRO-ALDOL CONDENSATION REACTION

This chapter of the thesis is divided into two sections describing the complete characterization of Ni and Co-based ternary LDHs synthesized via the simple co-precipitation method and their derived mixed oxides. The activity measurement of the precursor LDHs and their derived mixed oxides have been tested for solvent free base-catalysed organic reaction such as nitro-aldol condensation reaction under mild and microwave conditions.

5.1 Prologue

Nitro-aldol condensation reaction is one of the most important C–C bond formation reactions and commonly known as Henry reaction [1,2]. It is the combination of aldehyde or ketone with nitro-alkane in the presence of a base to form β -nitro-alkanols or 2-nitro-alkanols. The product finds importance in many syntheses that include synthesis of various important biological compounds [3,4]. Because of its great importance it is widely used in bulk and fine chemical industries [5]. The classical method for the synthesis of 2-nitro-alkanol involves the use of various bases including sodium hydroxide, sodium carbonate, bicarbonates etc. [6,7] as well as the use of hazardous solvents which causes environmental problem. The main drawback of the Henry reaction is its tendency to form side products, which include the formation of nitro-alkene by the elimination of water molecule and formation of self-condensation reaction product (Cannizzaro reaction) in case of sterically hindered substrate [5]. Therefore it is very much challenging to develop an economically viable and environmentally safer process for selective synthesis of 2-nitro-alkanol.

Microwave (MW) assisted reactions are environmentally benign reactions which have attracted greatest importance in the recent years [8]. These microwave assisted reactions provide simple process that minimizes the environmental harmfulness of classical reactions with enhanced reaction rates at shorter reaction time with greater selectivity of the desired product [9].

Due to the unique layered structure with surface hydroxyl groups, layered double hydroxides are widely adopted as solid base catalysts for a wide variety of organic transformations [10]. Another important property of LDH is anion exchange capacity [11] due to which, LDHs can be widely used in various fields such as catalysts and catalyst support [12–16]. The catalytic efficiency of binary LDHs can be further improved with ternary systems by incorporation of a third cation, such as M^{2+} ($M^{2+} = Ni^{2+}, Co^{2+}, Cu^{2+}, Zn^{2+}$ etc.) cations and/ or M^{3+} ($M^{3+} = Fe^{3+}, Cr^{3+}$ etc.) cations in the brucite-like LDH without affecting the structure of the layered material [17–19]. Furthermore, upon thermal treatment, LDHs can be converted into well-dispersed mixed metal oxides with various advantages of high surface area, thermal stability, and numerous Lewis base sites [20–22]. As a result, LDH catalysts have currently drawn considerable attention as environmentally benign heterogeneous solid base catalysts for various important organic reactions by replacing homogeneous catalysts [23–30].

Section 5A: Synthesis of high surface area mixed metal oxide from the NiMgAl LDH precursor for nitro-aldol condensation reaction

In this section, we have discussed the characterization and catalytic activity of various mixed oxides derived from MgAl, NiMgAl and CoMgAl LDHs synthesized via simple co-precipitation method. The activity of the LDH derived mixed oxides has been tested as base catalyst for solvent free nitro-aldol condensation reaction under mild condition. The synthetic procedures of catalysts, details of characterization techniques and catalytic reaction procedures were described in chapter 2.

5A.1 Results and discussion

5A.1.1 Characterization

Figure 5A.1a shows the powder XRD patterns of LDHs. The formation of hydroxalcalite (HT) like layered structure has been confirmed from the formation of sharp, highly intense peaks at low 2θ angles and comparatively broad, less intense peaks at higher 2θ angles which match well with previous reports [31,32]. In all cases, the diffraction peaks are observed approximately at $2\theta = 11.61, 23.41, 34.81, 38.81, 46.31, 60.85$ and 62.11° which can be assigned to (003), (006), (012), (015), (018), (110) and (113) reflections, respectively (JCPDS card no. 38-0478) [33]. The effect of partial substitution of Mg^{2+} ions with Ni^{2+} and Co^{2+} on the crystallization procedure is well reflected from the broad and less intense peaks of both CoMgAl and NiMgAl LDHs in comparison to MgAl LDH. The diffraction peaks corresponding to (015) and (018) reflections are not distinct in the case of NiMgAl, while the (015), (018), (110) and (013) reflections are completely disappeared in case of CoMgAl. This is due to the larger size of Co^{2+} (0.88 Å) and Ni^{2+} (0.83 Å) ions which could not be accommodated well in the brucite layers. The substitution effect can be understood well from the lattice parameters and crystallite sizes of the LDH samples. The lattice parameter ' a ' is a function of the average distance of metal ions within the brucite layers and it can be obtained from the (110) reflection peak. The ' c ' parameter is related to the thickness of the brucite-like layer and the interlayer distance which can be obtained from the (003) reflection peak [19]. The lattice parameters

' a ' ($a = 2d_{110}$) and ' c ' ($c = 3d_{003}$) have been calculated and are presented in Table 5A.1. It is observed that the lattice parameter ' a ' gradually increases in case of substituted LDHs and it is due to the increased metal–metal distance on partial substitution of metal cations in MgAl LDH. However, the lattice parameter ' c ' increases in case of NiMgAl LDH, but it decreases in CoMgAl LDH. This difference in ' c ' parameter can be attributed to the larger ionic radius of Co^{2+} (0.88 Å) compared to Ni^{2+} (0.83 Å) [31,32].

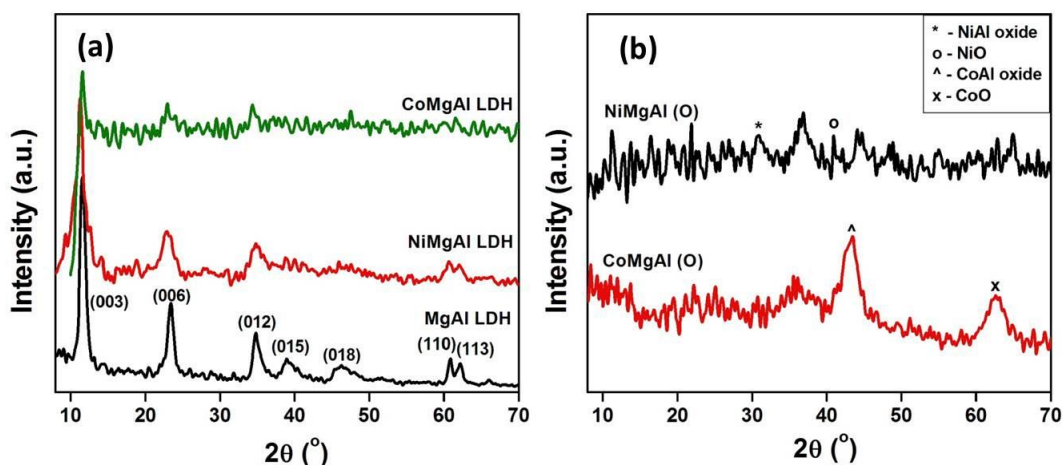


Figure 5A.1. X-ray powder diffraction patterns of a) MgAl, NiMgAl and CoMgAl LDHs and; (b) NiMgAl (O) and CoMgAl (O) mixed oxides.

Again, the crystallite sizes of NiMgAl and CoMgAl LDH are found to be less compared to MgAl LDH demonstrating the inclusion of larger cations in the brucite layers which results in the distortion of layered structure (Table 5A.1) [18]. The powder XRD patterns of the NiMgAl (O) and CoMgAl (O) mixed oxides are shown in Figure 5A.1b. The XRD patterns do not exhibit any characteristic diffraction peaks corresponding to LDH. This is because, on calcination at higher temperatures, the layered structure of the LDH materials get collapsed resulting in the conversion to their corresponding mixed oxides. In case of NiMgAl mixed oxide, the diffraction peaks observed at $2\theta = 16.4^\circ$ can be attributed to (001) reflection of $\theta\text{-Al}_2\text{O}_3$ (JCPDS card No. 86-1410); $2\theta = 21.85, 55.05$ and 64.95° are attributed to (200), (422) and (440) reflections, respectively of MgAl_2O_4 (JCPDS card No. 77-1193 and 82-2424); $2\theta = 26.9^\circ$ is attributed to (111) reflection of AlO (JCPDS card No. 75-0278); $2\theta = 30.9^\circ$ is attributed to (220) reflection of $(\text{Ni}_{0.198}\text{Al}_{0.802})(\text{Al}_{1.198}\text{Ni}_{0.802})\text{O}_4$ (JCPDS card No. 81-0718); $2\theta = 36.85$ and 62.1° are attributed to (111) and (220)

reflections of MgO (JCPDS card No. 89-7746 and 79-0612); $2\theta = 44.1^\circ$ is attributed to (012) reflection of NiO (JCPDS card No. 89-7390); $2\theta = 48.85^\circ$ is attributed to (133) reflection of $k\text{-Al}_2\text{O}_3$ (JCPDS card No. 88-0107) and $2\theta = 52.7^\circ$ is attributed to (511) reflection of $\text{Mg}_{0.36}\text{Al}_{2.44}\text{O}_4$ (JCPDS card No. 77-0729). In case of CoMgAl mixed oxide, the diffraction peaks observed at $2\theta = 12^\circ$ is attributed to (110) reflection of $\text{Al}_{12}\text{Mg}_{17}$ (JCPDS card No. 73-1148); $2\theta = 22.2$ and 43.45° are due to $\text{Co}_6\text{Al}_2\text{O}_{11}$ (JCPDS card No. 51-0041); $2\theta = 25.1^\circ$ is attributed to (012) reflection of Al_2O_3 (JCPDS card No. 89-3072); $2\theta = 35.55^\circ$ is attributed to (222) reflection of $\text{Mg}_{0.36}\text{Al}_{2.44}\text{O}_4$ (JCPDS card No.77-0729) and $2\theta = 62.6^\circ$ is attributed to (112) reflection of CoO (JCPDS card No.65-5474).

The chemical composition of the LDH samples have been determined from the elemental analyses and presented in Table 5A.1. It is observed that the molar ratio of $\text{M}^{2+}\text{Mg}/\text{Al}$ is close to 3 and that of M^{2+}/Mg ($\text{M}^{2+} = \text{Ni}^{2+}$ or Co^{2+}) is 1:1 which is nearly the same as that of the starting solution.

Table 5A.1. Chemical composition, crystallographic data and crystallite size of mixed oxides.

Catalysts	Atomic ratio		d_{003} (Å)	d_{110} (Å)	Cell parameters(Å)		Crystallite size (Å)	
	Starting	Analyzed [#]			<i>c</i>	<i>a</i>	003	110
MgAl	3:1	3:0.9	7.69	1.52	23.07	3.04	90	134
Ni ²⁺ MgAl	1.5:1.5:1	1.5:1.47:0.9	7.87	1.53	23.61	3.05	63.5	113
Co ²⁺ MgAl	1.5:1.5:1	1.5:1.48:1	7.68	1.55	23.04	3.09	54	70

[#] Determined by ICP

Figure 5A.2a shows the FTIR spectra of LDHs. The absorption bands observed nearly at 3478.2 and 1662.9 cm^{-1} can be assigned to the stretching and bending vibrations of the $-\text{OH}$ group of LDH layers and the interlayer water molecules [32, 19]. The sharp band observed around 1388.5 cm^{-1} is attributed to the asymmetric stretching of the CO_3^{2-} ions. Broad bands are observed below 1000 cm^{-1} (around $500\text{--}800\text{ cm}^{-1}$), which corresponds to $\text{M}\text{--}\text{O}$ vibrations [19]. In case of LDH derived mixed oxides in Figure 5A.2b, the bands observed around 555.3 and 671.9 cm^{-1} correspond to the vibration of the

metal–oxygen (M–O) bond. Moreover, the band observed around 1374.9 cm^{-1} is due to the carbonate which may arise from the adsorption of carbon dioxide from air on the surface of the metal oxides [32].

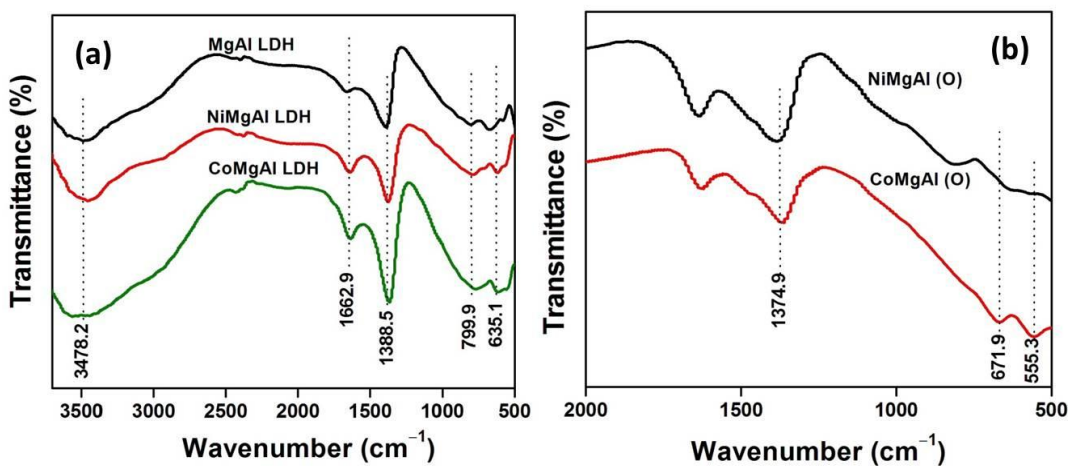


Figure 5A.2. FTIR spectra of (a) MgAl, NiMgAl and CoMgAl LDHs; and (b) NiMgAl (O) and CoMgAl (O) mixed oxides.

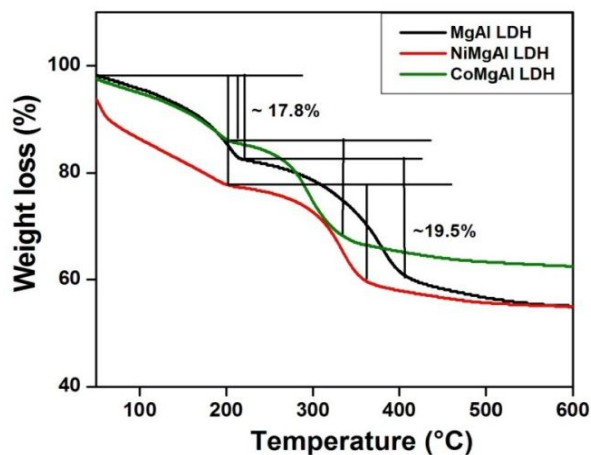


Figure 5A.3. TGA curves of MgAl, NiMgAl and CoMgAl LDHs.

The thermogravimetric analyses of the precursor LDHs have been carried out before calcination. Figure 5A.3 shows the TGA thermograph of the LDH samples possessing two major weight loss steps. The first weight-loss is observed in the temperature range of $50\text{--}200\text{ }^{\circ}\text{C}$ with a weight loss of $\sim 17.8\%$, corresponding to the removal of surface and interlayer water molecules. The second weight-loss step observed

in the temperature range of 250–400 °C with a weight-loss of ~19.5% is due to the dehydroxylation of the brucite layer as well as the decomposition of the carbonate anions [34].

The SEM images of the LDH samples are shown in Figure 5A.4. Flat plate like shapes is observed in case of MgAl LDH. Whereas, in case of NiMgAl and CoMgAl LDH, crystallites with large irregular particle sizes are observed which are due to agglomeration of Mg^{2+} with M^{2+} ($M^{2+} = Ni^{2+}$ or Co^{2+}) in MgAl LDH.

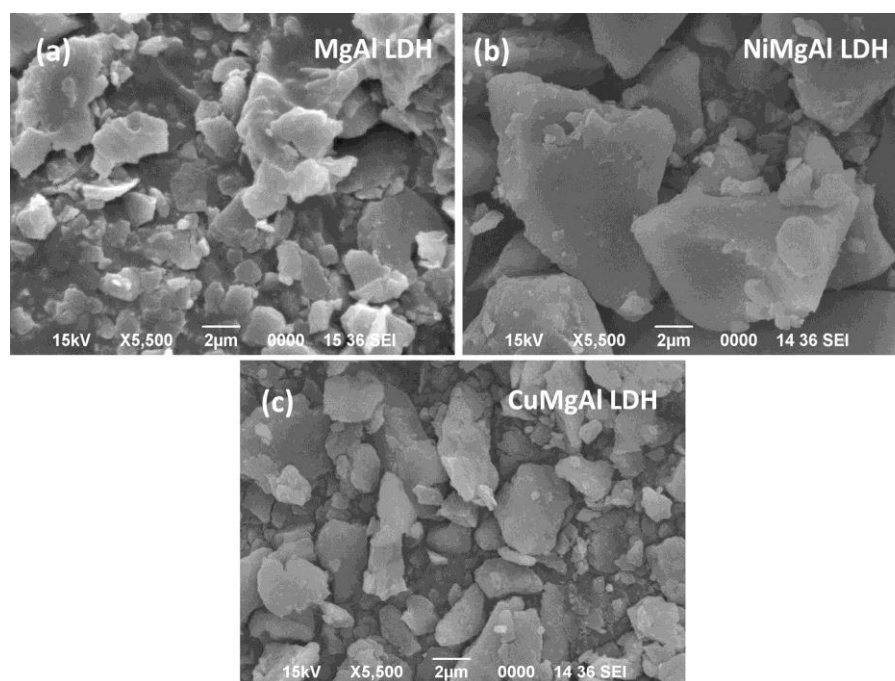


Figure 5A.4. SEM images of (a) MgAl, (b) NiMgAl and (c) CoMgAl LDHs.

The porosity of the LDHs derived mixed oxides has been investigated by using N_2 adsorption–desorption measurements. Figure 5A.5 (a and b) shows the N_2 adsorption–desorption isotherm and pore size distribution curve of LDH derived mixed oxides, respectively. It is observed that NiMgAl mixed oxide exhibits isotherm of type IV with hysteresis loop H1, which is the characteristic of mesoporous material with regular pore structure [35]. The average pore size is around 49.6 Å (Figure 5A.5b). While, MgAl and CoMgAl mixed oxides exhibit isotherm of type IV with combination of hysteresis loops H1 and H3 [36,37] and possess an average pore size of around 88 and 107 Å, respectively (Figure 5A.5b). The calculated BET surface areas (S_{BET}) and pore volumes of LDH

derived mixed oxides are summarized in Table 5A.2. From the table, it is observed that NiMgAl mixed oxide possesses the highest BET surface area of 753 m²/g with pore volume of 1.279 cm³/g. While in the case of MgAl and CoMgAl mixed oxides, the observed surface area are 561 m²/g and 401 m²/g; and pore volume are 0.974 cm³/g and 0.937 cm³/g, respectively. The high BET surface area and the pore volume of the mixed oxides are due to the removal of adsorbed and interlayer water molecules and carbonate ions from the LDH layers at high temperature.

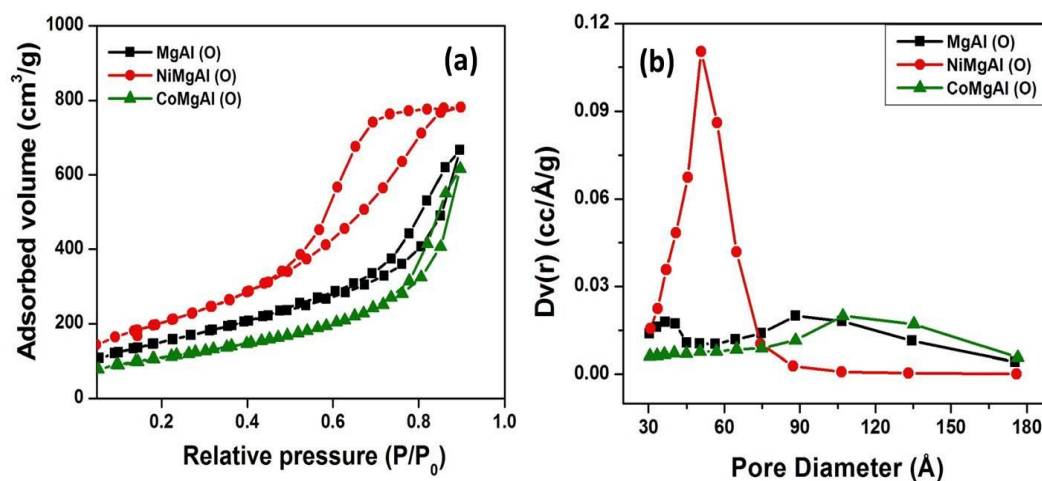


Figure 5A.5. (a) N₂ adsorption-desorption isotherms and (b) pore size distribution curves of MgAl (O), NiMgAl (O) and CoMgAl (O) mixed oxides.

Table 5A.2. Textural properties of LDH derived mixed oxides.

Entry	Catalysts	S_{BET} (m ² /g)	Pore Volume (cm ³ /g)	Pore Diameter (Å)
1	MgAl (O)	561	0.974	88
2	NiMgAl (O)	753	1.279	51
3	CoMgAl (O)	401	0.937	107

5A.1.2 Catalytic performance

The catalytic activity of the LDHs and their derived mixed oxides has been employed for the nitro-aldol condensation reaction. We first carried out the reaction under solvent free

conditions by taking a 1:10 molar ratio of 4-nitrobenzaldehyde and nitromethane in a mmol scale with 10 mg of the catalyst at room temperature. The isolation of the products was carried out with the help of thin layer chromatography and conversions (%) were determined from ^1H NMR data of crude mixture. Table 5A.3 shows the nitroalkylation of 4-nitrobenzaldehyde with nitromethane over various catalysts at room temperature.

Table 5A.3. Nitroalkylation of 4-nitrobenzaldehyde with nitromethane over various catalysts at room temperature^a

Entry	Catalysts	Time (h)	Conversion (%) ^b
1	MgAl LDH	12	86
2	NiMgAl LDH	8	91
3	CoMgAl LDH	10	84
4	MgAl (O)	6	95
5	NiMgAl (O)	2	99
6	CoMgAl (O)	4	97

^aReactions were carried out with a 1:10 molar ratio in a 1 mmol scale of 4-nitrobenzaldehyde and nitromethane using 10 mg catalyst. ^bDetermined from ^1H NMR data of crude mixture.

A good to excellent conversion to the product is obtained (84–91%) for all the uncalcined catalysts, but the time taken to complete the reactions is more (8–10h). Moreover, we have observed that partial substitution of metal ions in MgAl LDH further improve the catalytic activity. This increase in catalytic activity on partial substitution of metal ions can be explained on the basis of increased cell parameters ‘*a*’ and ‘*c*’ in case of NiMgAl and CoMgAl LDH (Table 5A.1). The increased value of *d*-spacing in case of NiMgAl LDH ($d_{003} = 7.87 \text{ \AA}$) can be attributed to the superior catalytic activity of the catalyst for nitro-adol condensation reaction by providing increased basal spacing for the reaction to take place within the layers. However, performing the reaction with calcined LDHs under the similar reaction conditions, it is observed that the reaction is much faster than the uncalcined LDHs resulting 95–99% conversion of the product within 2–6 hrs with 100% selectivity. Therefore, calcined catalysts have preferred over the uncalcined ones and further studies have been employed by using the mixed oxides. Table 5A.3 also shows

that for both cases (uncalcined and calcined), NiMgAl LDH and NiMgAl (O) mixed oxide are the most efficient catalysts compared to that of MgAl and CoMgAl (entries 2 and 5.). The high BET surface area and the large pore volume of the NiMgAl mixed oxide (Figure 5A.5) results in the superiority of its catalytic activity over the other two mixed oxides for nitro-aldol condensation reaction. Therefore, NiMgAl mixed oxide has been considered as the best catalyst in this study.

After finding the best catalyst from our observation, we have studied the effect of various reaction parameters to optimize the reaction conditions for nitro-aldol condensation reaction. At first, we studied the effect of temperature on the reaction by varying the reaction temperature from 25 °C (RT) to 60 °C and the results are summarized in Table 5A.4. It is observed that on increasing the temperature upto 60 °C, the reaction time decreases from 2h to 30 min. However, temperature does not show great impact over the conversion (%) and we observe almost a similar type of conversion in all cases. Therefore, it is convenient to use the greener path. So, further studies have been performed at room temperature under solvent free conditions.

Table 5A.4. Effect of temperature on nitro-aldol condensation reaction of 4-nitrobenzaldehyde and nitromethane catalyzed by NiMgAl mixed oxide^a

Entry	Temperature (°C)	Time (h)	Conversion (%) ^b
1	RT	2	99
2	40	1	98
3	60	30 min	99

^aReactions were carried out with 1:10 molar ratio in 1 mmol scale of 4-nitrobenzaldehyde and nitromethane using 10 mg catalyst. ^bDetermined from ¹H NMR data of crude mixture.

We have next studied the effect of catalyst amount (NiMgAl mixed oxide) on percentage conversion of the nitro-aldol reaction with time (Table 5A.5). Here, we have selected four catalyst amounts such as 5, 10, 15 and 20 mg under similar reaction conditions. Upon increasing the catalyst amount from 5 to 15 mg, the conversion (%) increases along with decrease in the reaction time. Further, increase in the catalyst amount

to 20 mg, the reaction completes within 1h but the conversion (%) is almost similar. So, we have selected 10 mg as our optimum catalyst amount for further studies at room temperature under solvent free conditions.

Table 5A.5. Effect of catalyst amount (NiMgAl mixed oxide) on nitro-aldol condensation reaction of 4-nitrobenzaldehyde and nitromethane^a

Entry	Catalyst amount (mg)	Time (h)	Conversion (%) ^b
1	5	4	95
2	10	2	99
3	15	2	98
4	20	1	99

^aReactions were carried out with 1:10 molar ratio in 1 mmol scale of 4-nitrobenzaldehyde and nitromethane using 10 mg catalyst. ^bDetermined from ¹H NMR data of crude mixture.

Table 5A.6. Nitro-aldol condensation reaction of nitromethane with different aldehydes using NiMgAl (O) mixed oxide.

Entry	Substrate	Time (h)	Conversion (%) ^a
1	4-nitrobenzaldehyde	2	99 ^b
2	2-nitrobenzaldehyde	4	98
3	3-nitrobenzaldehyde	4	97
4	1-naphthaldehyde	20	76
5	Furfuraldehyde	20	70
6	4-hydroxybenzaldehyde	36	80
7	4-methylbenzaldehyde	36	78
8	4-chloroaldehyde	36	91

^a Determined by ¹H NMR data of crude mixture. ^b Isolated pure product.

After getting optimizing conditions for nitro-aldol condensation reaction, the reaction has been performed with a variety of aldehydes, e.g. simple aromatic aldehydes, heterocyclic aldehydes and polycyclic aromatic aldehydes (Table 5A.6). It is observed from the table that by changing the substituents, the conversions (%) are also getting

changed. As expected, substrates with electron withdrawing groups give higher % conversion (97–99%, entries 1–3), while the % conversion decreases (80–91%) in case of the substrate with electron donating groups (entries 6–8). However, it is also observed from the table that the reaction with polycyclic aldehydes gives better % conversion of 70–76% (entries 4 and 5) within a time period of 20h.

Comparing our results with the reported one, we have observed that NiMgAl (O) mixed oxide is an efficient catalyst for nitro-aldol (Henry) reaction. Cwik *et al.* [38] carried out nitroaldol-reaction of aldehydes in the presence of non-activated Mg:Al 2:1 hydrotalcite. The reaction was performed at room temperature in methanol, tetrahydrofuran and nitromethane and best results were observed using nitromethane as solvent (20 mol equivalent). However, conversion was 95% in 5h. Manikandan *et al.* [39] reported the synthesis and spectral characterization of three new nickel(II) complexes containing pyridoxal N(4)-substituted thiosemicarbazone ligands with triphenylphosphine. The new nickel (II) complexes were used as catalysts in the nitroaldol (Henry) reaction by employing various aldehydes with nitromethane in an ionic liquid medium. The reaction was carried out at room temperature for 5h and the yield was observed to be about 52%. However, upon using ionic liquid as solvent medium, a slight improvement in the yield was observed from 52 to 64%. The maximum yield of 92% was observed in 12h at a 3.0 mmol concentration of the catalyst in 2 mL of methanol. Sutradhar *et al.* [40] synthesized a new cyclic binuclear Ni(II) complex, $[\text{Ni}_2(\text{H}_2\text{L})_2] \cdot 4\text{MeOH}$ using the Schiff base N^1, N^3 -bis(2-hydroxybenzylidene) malonohydrazide (H_4L). A maximum conversion of *ca.* 93% was obtained at 60 °C, for a 24h reaction time, with 1 mol% loading of the catalyst with the good syn:anti molar ratio of 72:28.

The effect of calcination temperature on catalytic activity under optimum reaction conditions has been studied and the results are shown in Table 5A.7. We have calcined the catalyst at a lower (350 °C) and at a higher (550 °C) calcination temperature to the reported one (450 °C). The sample calcined at 350 °C, shows low catalytic activity with 84% conversion in 6h. This is because, calcination at lower temperature leads to no characteristic change in the LDH structure. It can be considered as a dehydrated one with its basic sites occupied by CO_3^{2-} ions. Consequently, the BET surface area of the catalyst

is relatively lower ($584 \text{ m}^2/\text{g}$) resulting in the lower catalytic activity. On the other hand, the sample calcined at $550 \text{ }^\circ\text{C}$, also exhibits lower catalytic activity with 86% conversion in 8h (Table 5A.7).

Table 5A.7. Effect of calcination temperature on nitro-aldol condensation reaction of 4-nitrobenzaldehyde and nitromethane catalyzed by NiMgAl (O) mixed oxide ^a

Entry	Calcination Temperature ($^\circ\text{C}$)	Time (h)	Conversion (%) ^b
1	350	6	84
2	450	2	99
3	550	8	86

^aReactions were carried out with 1:10 molar ratio in 1 mmol scale of 4-nitrobenzaldehyde and nitromethane using 10 mg catalyst. ^bDetermined from ^1H NMR data of crude mixture.

This is because the high calcination temperature leads to the phase transformation of mixed oxides into crystalline spinel phases which results in the lower BET surface area ($566 \text{ m}^2/\text{g}$) lowering the catalytic activity [41–46]. Figure 5A.6 shows the N_2 adsorption-desorption isotherm of NiMgAl (O) calcined at 350 and $550 \text{ }^\circ\text{C}$ which also exhibits isotherm of type IV. The basic sites formed after calcination of LDHs at $450 \text{ }^\circ\text{C}$ have been considered as the active sites in mixed metal oxides. The presence of different types of basic sites is related to $-\text{OH}$ groups, $\text{O}^{2-}-\text{M}^{\text{n}+}$ pairs and O^{2-} anions [20,47–51].

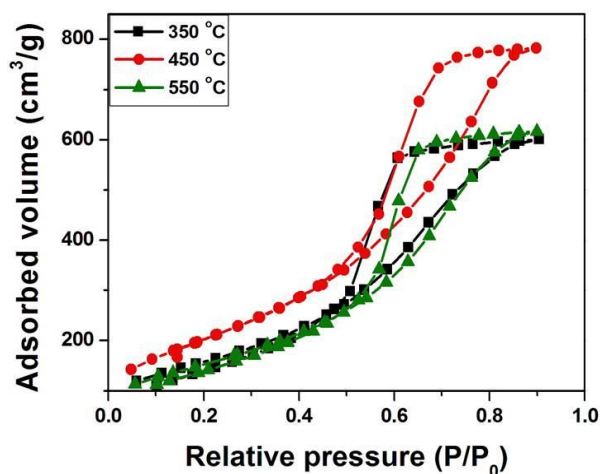


Figure 5A.6. N_2 adsorption-desorption isotherms of NiMgAl (O) mixed oxide at different calcination temperatures.

In order to better understand the reason behind the excellent catalytic activity of NiMgAl (O) mixed oxide, we have also performed the turnover frequency (TOF) measurement of the LDH derived mixed metal oxides and the results are displayed in Figure 5A.7. It is seen that the TOF increases in case of substituted catalysts than the unsubstituted one. The TOF is maximum for NiMgAl (O) mixed oxide (149 h^{-1}). While in the case of MgAl (O) and CoMgAl (O), the TOF are 12.5 and 36 h^{-1} , respectively, which are almost 11 and 4 times less than NiMgAl (O). Thus, the increase in TOF reflects the better catalytic performance of NiMgAl (O) mixed oxides for nitro-aldol condensation reaction.

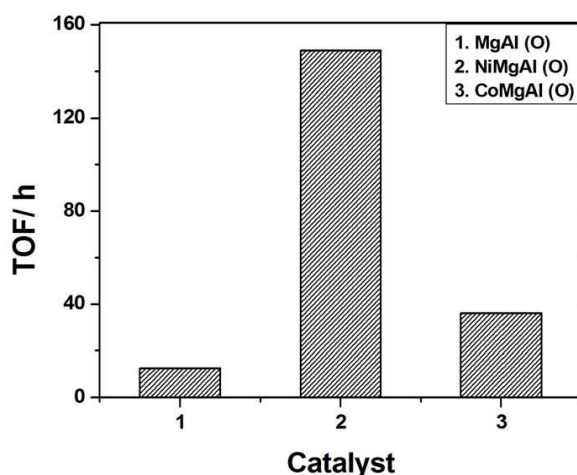


Figure 5A.7. Turnover frequency (TOF) of MgAl (O), NiMgAl (O) and CoMgAl (O) mixed oxides.

After testing the catalytic activity, it is important to check the recyclability of the catalyst for their practical application. To test the recyclability of the catalyst, we performed the condensation reaction upto four cycles employing 10 mg of the regenerated catalyst under similar experimental conditions and presented in Table 5A.8. When the regenerated catalyst is subjected for another fresh cycle, it takes 2h to complete the reaction with conversion 96% (entry 1). Similarly, it is observed that upto 3rd cycles, the catalyst retains its activity above 90%, but, the time required to complete the reaction become high (3–4h, entries 2 and 3). Thus, the catalyst, NiMgAl (O) mixed oxide becomes active upto four cycles (including the fresh one) without any significant loss in the catalytic activity. The reason for the slight decrease in the catalytic activity of the

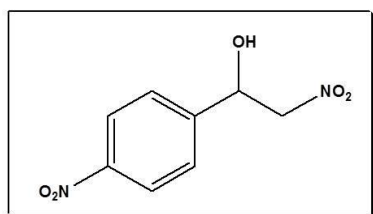
catalyst is due to the loss of catalyst during separation or deactivation of the active sites in the catalyst. The leaching of metals during recyclability of catalyst was also studied. For this test, 1 mmol 4-nitrobenzaldehyde, 10 mmol nitromethane and 10 mg of the catalyst were taken in a round bottomed flask and stirred for 1h at room temperature without any solvent. The catalyst was then filtered off and the experiment was continued with the filtrate for upto 24h. It was observed that the conversion remained unchanged indicating the absence of any metal in the filtrate.

Table 5A.8. Recyclability of NiMgAl (O) mixed oxide.

Entry	No. of cycle	Time (h)	Conversion(%) ^a
1	1 st run	2	96
2	2 nd run	3	95
3	3 rd run	4	92

^a Determined from ¹H NMR data of crude mixture.

Spectral data



2-Nitro-1-(4-nitrophenyl) ethan-1-ol

¹H NMR (400 MHz, CDCl₃): δ 3.75 (s, 1 H), δ 4.58-4.61 (m, 2H), δ 5.60-5.62 (m, 1H), δ 7.64(d, J_{HH} = 8.7 Hz, 2H), 8.27 (d, J_{HH} = 9.2 Hz, 2H); ¹³C NMR (100 MHz CDCl₃): δ 0.0, 80.8, 124.2, 127.0, 145.4, 148.2 ppm.

The ¹H and ¹³C NMR spectra of 2-Nitro-1-(4-nitrophenyl) ethan-1-ol are shown in Image A.1 and A.2 of Appendix.

In summary, we have synthesized high surface area mixed metal oxides from their precursor LDHs and also observed the influence of divalent metal cations on structural property and catalytic activity of MgAl LDH. The XRD patterns of all the as prepared LDHs reveal the formation of hydrotalcite (HT) type layered structure. The partial substitution of Mg²⁺ ions with Ni²⁺ and Co²⁺ affects the crystallization procedure which is well reflected from the broad and less intense peaks of both CoMgAl and NiMgAl

samples in comparison to MgAl sample. The formation of mixed oxides is revealed from the powder XRD patterns which possess no characteristic peaks that corresponding to LDH. The mixed metal oxides are found to be catalytically more active towards nitro-aldol condensation reaction under solvent free condition at room temperature. The high catalytic activity of NiMgAl (O) mixed oxide is attributed to the high BET surface area (753 m²/g) and TOF. Moreover, the catalyst, NiMgAl (O) mixed oxide shows reusability upto 4th cycle without any characteristics loss in its activity.

Section 5B: Effect of Ni on structural properties of NiMgAl-LDH derived mixed oxides and their catalytic activity for nitro-aldol condensation reaction

This section describes the complete characterization of various mixed oxides derived from NiMgAl LDHs with variable composition synthesized via co-precipitation method. The LDH derived mixed oxides have been employed as base catalyst for nitro-aldol condensation reaction under solvent free microwave conditions. The synthetic procedures of precursor LDHs with variable composition and their derived mixed oxides are described in section 2.2.1 and 2.2.6 of Chapter 2. The detailed characterization techniques and catalytic reaction procedures are also discussed in Chapter 2.

5B.1 Results and discussion

5B.1.1 Characterization

Figure 5B.1a shows the powder XRD patterns of precursor NiMgAl LDHs with variable composition of Ni, keeping the molar ratio of $(\text{Ni}^{2+} + \text{Mg}^{2+})/\text{Al}^{3+} = 3$. XRD patterns of all the samples exhibit sharp and intense peaks at low 2θ angles and broad, less intense peaks at higher 2θ angles which reveal the characteristics of hydrotalcite-like LDH that match well with the XRD database (JCPDS card no. 38-0478). In case of all the samples, the diffraction peaks are observed due to (003), (006), (012), (015), (018), (110) and (113) reflections, approximately at $2\theta = 11.6, 23.4, 34.8, 38.8, 46.3, 60.85$ and 62.1° . The substitution of Mg^{2+} with Ni^{2+} cation in MgAl LDH is well reflected from the XRD patterns. Less intense peaks are observed in case of Ni substituted precursor samples (LDH2 to LDH5) as compared to that of LDH1 (without Ni). The intensity difference of the peaks on Ni^{2+} substitution is ascribed due to the presence of $\text{Ni}(\text{OH})_2$ phases resulting in the formation of secondary crystalline phase [52]. On thermal treatment, the precursor LDHs have been converted into their corresponding mixed metal oxides, which are clearly depicted from the powder XRD patterns (Figure 5B.1b). The XRD patterns show that there is no characteristic peak corresponding to LDHs. The (003) plane is completely disappeared in the entire samples. Calcination at higher temperature, leads to the distortion of the layered structure of LDHs, converting them into their corresponding

mixed metal oxides. In case of LDH1 (O), the diffraction peaks observed at $2\theta = 43.4$ and 63.1° are due to (220) reflections of MgO (JCPDS card No. 89-4248 and 79-0612). The diffraction peak observed at $2\theta = 36.1$ for LDH2 (O), LDH3 (O) and LDH4 (O) mixed oxides are due to (311) reflection of MgAl_2O_4 (JCPDS card No. 82-2424); while the peaks at $2\theta = 43.4$ and 62.8° are attributed to (012) and (111) reflection of NiO, respectively (JCPDS card No. 89-7390 and 89-7131). Moreover, the peaks at $2\theta = 43.4$ and 62.8° are also attributed to (220) reflection of MgO (JCPDS card No. 89-4248 and 79-0612). In case of LDH5 (O), the diffraction peaks observed at $2\theta = 36.1, 43.1$ and 62.9° are ascribed due to (101/003), (012) and (111) reflections of NiO, respectively (JCPDS card No. 89-7131, 89-7390 and 89-7131).

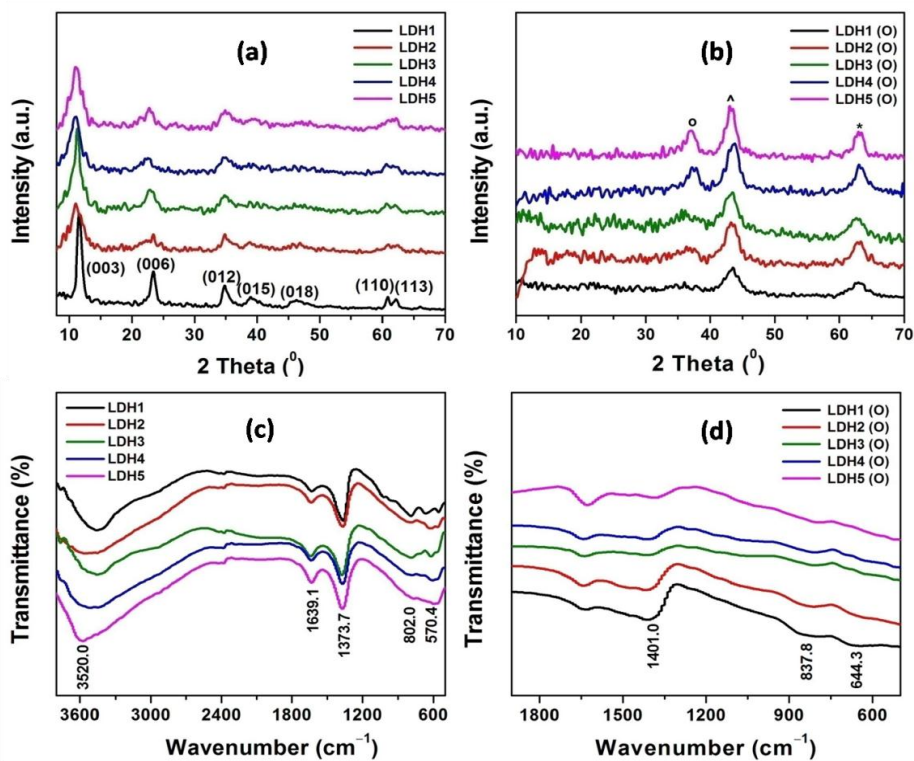


Figure 5B.1. Powder XRD patterns of (a) LDHs and (b) LDH derived mixed oxides (o – NiO, * - MgO and ^ - MgAl_2O_4); and FTIR spectra of (c) LDHs and (d) LDH derived mixed oxides.

Figure 5B.1c shows the FTIR spectra of precursor LDHs. The bands around 3520.0 cm^{-1} are assigned to the stretching vibration of hydroxyl group of layers and water

molecules in the interlayer region of LDH. The weak bands near 1639.1 cm^{-1} are assigned to the $-\text{OH}$ bending vibration of water molecules. The bands observed around 1373.7 cm^{-1} are due to the presence of carbonate anion (CO_3^{2-}). However, the bands below 1000 cm^{-1} are associated with the $\text{M}-\text{O}$ vibrations. Figure 5B.1d shows the FTIR spectra of the LDH derived mixed oxides. The bands observed near at 644.3 and 837.8 cm^{-1} are attributed to the vibration of metal–oxygen ($\text{M}-\text{O}$) bond of the mixed oxides. Moreover, small and weak bands around 1401.0 cm^{-1} are also observed in case of the entire samples are assigned to the carbonate ion due to the adsorption of carbon dioxide from air on the surface of the metal oxides [32].

The thermal stability of the precursor LDHs have been analysed before calcination through thermogravimetric analysis and respective thermograms are shown in Figure 5B.2. Two weight loss steps are mainly observed in case of all the samples that are typical of LDH materials. The first weight-loss is observed in the temperature range of $50\text{--}200\text{ }^\circ\text{C}$, which is attributed to the removal of water molecules adsorbed on the surface and in the interlayer region of LDHs. The second weight-loss step observed between temperature ranges of $250\text{--}400\text{ }^\circ\text{C}$ is due to the dehydroxylation of the brucite layer as well as the decomposition of the carbonate anions [19,53].

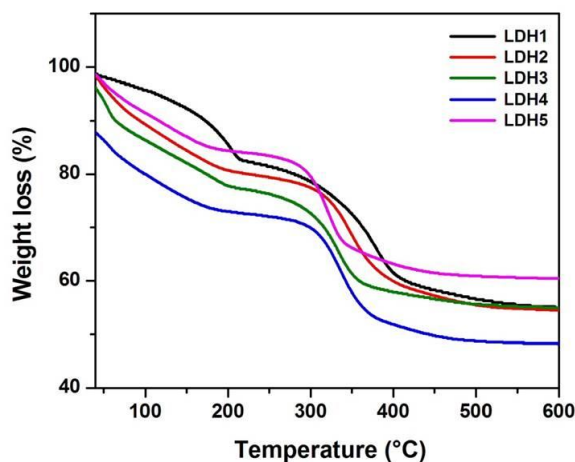


Figure 5B.2. Thermogravimetric analysis curves of LDHs.

The chemical analyses of the precursor LDHs have been carried out and it is observed that the molar ratios of the binary cations ($\text{Ni}^{2+}/\text{Mg}^{2+}$) in the precursor LDHs are

same as that of the starting solution and ratio of $(\text{Ni}^{2+} + \text{Mg}^{2+})/\text{Al}^{3+} = 3$ (Table 5B.1).

Table 5B.1. Chemical analyses of the precursor LDHs.

LDHs	$\text{Ni}^{2+}:\text{Mg}^{2+}:\text{Al}^{3+}$ ratio	
	Starting	Analyzed ^a
LDH1	0: 3: 1	0: 3: 0.9
LDH2	1: 2: 1	1: 2: 1
LDH3	1.5: 1.5: 1	1.5:1.47:0.9
LDH4	2: 1: 1	2: 0.9: 1
LDH5	3: 0: 1	3: 0: 1

^a Determined by AAS

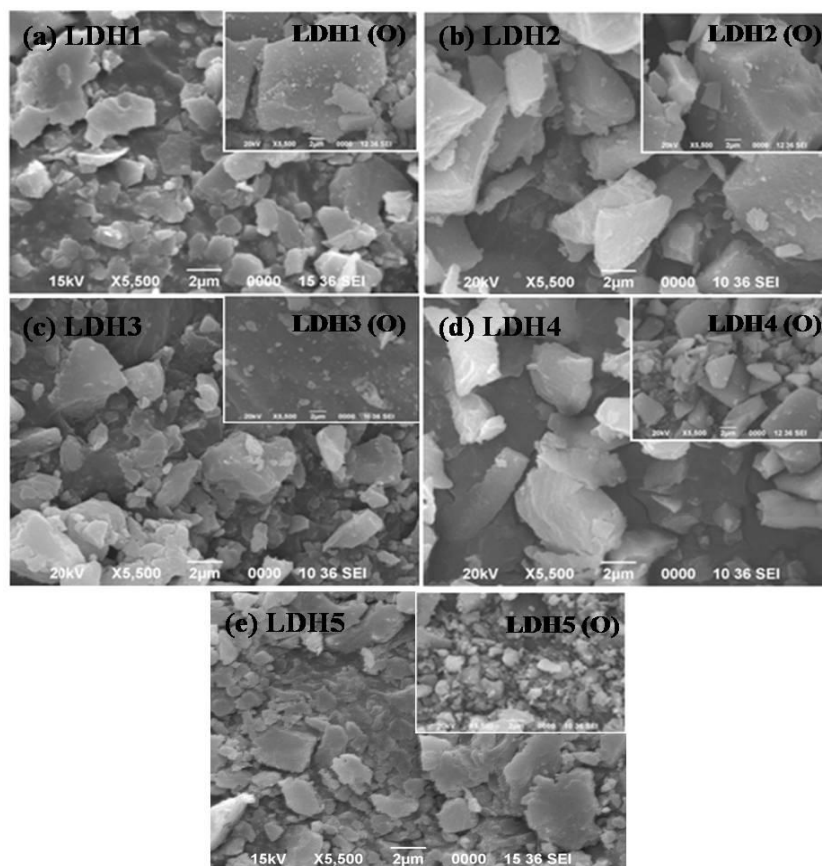


Figure 5B.3. SEM images of LDHs and inset shows for LDH derived mixed oxides.

Figure 5B.3 shows the SEM images of precursor LDHs and insets are for LDH derived

mixed oxides. Crystallites with flat plate-like shapes are observed in case of binary LDH1 (without Ni) and LDH5 (without Mg). However, in case of ternary LDHs (LDH2, LDH3 and LDH4), no distinct shape is observed. This is because agglomeration takes place on substitution of Mg^{2+} with Ni^{2+} ion in MgAl LDH and thereby results in the formation of crystallites with large irregular particle size. The SEM images of mixed oxide (inset of Figures) show that the crystallites with flat plate like shapes as well as crystallites with large particle size get destroyed upon calcination at high temperature.

Figure 5B.4 shows the N_2 adsorption-desorption isotherms of LDH derived mixed oxides. All the samples exhibit the characteristic of mesoporous material by showing the type IV isotherm [43]. However, the mixed oxide, LDH1 (O) exhibits isotherm with combination of hysteresis loop H1 and H3 and the other four exhibit isotherm with hysteresis loop of type H1 corresponding to regular pore structure [44]. The BET surface area, pore volume and pore diameter of all the mixed oxides have been calculated and are summarized in Table 5B.2. It is observed that BET surface area value goes on increasing with Ni content from LDH1 (O) to LDH3 (O). However, further increase in Ni content, the surface area value gradually decreases (entries 4 and 5, Table 5B.2). This observation can be ascribed due to the larger ionic radius of Ni^{2+} (0.83 Å) compared to Mg^{2+} (0.72 Å) ion.

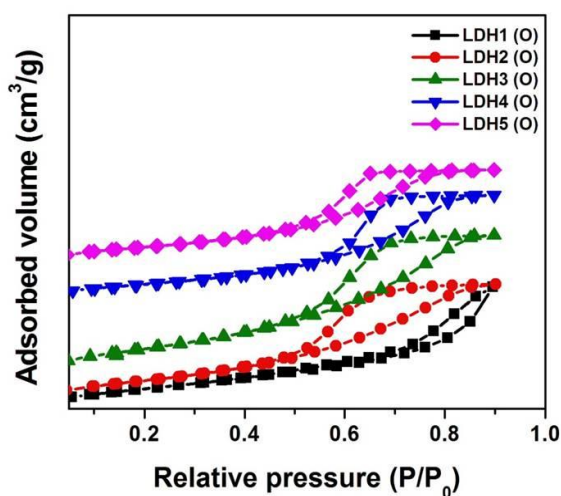


Figure 5B.4. N_2 adsorption-desorption isotherms of LDH derived mixed oxides.

Due to its larger size, inclusion of higher content of Ni^{2+} cation further inhibit the well accommodation of Ni^{2+} inside the brucite-like layers and hence smaller amount of Ni^{2+} cations are incorporated into LDH matrix; consequently, lowering the surface area of their derived mixed oxides. The mixed oxide, LDH3 (O) with equimolar mixture of Ni^{2+} and Mg^{2+} (1:1) possesses the highest BET surface area of $753 \text{ m}^2/\text{g}$ and pore volume $1.28 \text{ cm}^3/\text{g}$, but with lowest pore diameter that corresponds to the highly porous material with large number of pores. The observed BET surface area (S_{BET}) in case of other four samples are 561, 606, 480 and $454 \text{ m}^2/\text{g}$ for LDH1 (O), LDH2 (O), LDH4 (O) and LDH5 (O); with pore volume of 0.97, 1.11, 1.00 and $0.90 \text{ cm}^3/\text{g}$, respectively (Table 5B.2).

Table 5B.2. Textural properties of various mixed oxides derived from LDHs.

Entry	Samples	S_{BET} (m^2/g)	Pore Volume (cm^3/g)	Pore Diameter (nm)
1	LDH1 (O)	561	0.97	8.82
2	LDH2 (O)	606	1.11	5.04
3	LDH3 (O)	753	1.28	5.08
4	LDH4 (O)	480	1.00	5.71
5	LDH5 (O)	454	0.90	5.08

5B.1.2 Catalytic performance

Catalytic performances of the LDH derived mixed oxides were carried out for nitro-aldol condensation reaction under solvent free MW condition. All the reactions were carried out using 40% MW power at a temperature of $50 \text{ }^\circ\text{C}$ with 1:10 molar ratio of aldehyde and nitromethane (mmol scale) in a long necked microwave flask under refluxing condition. The reactions were first employed with the catalyst, LDH1 (O). For this purpose, we have taken 1 mmol of 4-nitrobenzaldehyde and 10 mmol of nitromethane using 10 mg of the catalyst. The conversion (%) of the products has been obtained from ^1H NMR data of crude mixture and is presented in Table 5B.3. The catalyst, LDH1 (O) exhibits conversion of 90% in 13 min (entry 1). After that we have performed the reaction under the same reaction conditions using other four catalysts. In case of ternary mixed oxides, LDH2 (O),

LDH3 (O) and LDH4 (O), improvement over the percentage conversion has been observed from 94 to 97 with decrease in the reaction time 12 to 7 min (entries 2–4). However in case of LDH5 (O), the % conversion is very low (81%) and the time required is also high (25 min, entry 5) compared to that of other four catalysts. Thus, the observation shows that ternary oxides (entries 2–4) display better catalytic performance over the binary oxides (entry 1 and 5) for nitro-aldol reaction. It is also observed that the molar ratio of divalent cations ($\text{Ni}^{2+}/\text{Mg}^{2+}$) in LDH precursors, greatly influence the catalytic activity of ternary oxides. The ternary oxide LDH3 (O) is found to be catalytically more active with 97% conversion in 7 min and 100% selectivity. The superior activity of LDH3 (O) is attributed to the presence of equivalent molar ratio of divalent metal cations ($\text{Ni}^{2+}/\text{Mg}^{2+} = 1$) and high BET surface area ($753 \text{ m}^2/\text{g}$) of the catalyst. Therefore, LDH3 (O) was preferred over all the other four catalysts for further study.

Table 5B.3. Nitro-aldol condensation of 4-nitrobenzaldehyde with nitromethane over various mixed oxides derived from LDHs ^a.

Entry	Catalysts	Time (min)	Conversion (%) ^b
1	LDH1(O)	13	90
2	LDH2(O)	10	94
3	LDH3(O)	7	97
4	LDH4(O)	12	95
5	LDH5(O)	25	81

^aReaction condition: 1 mmol aldehyde, 10 mmol nitromethane, 10 mg catalyst, 40% MW power (280 Watt), Temperature 50 °C. ^bDetermined from ¹H NMR data of crude mixture.

After getting the best catalyst from our observation, the next step was to optimise the reaction conditions by changing various reaction parameters such as catalysts amount, MW power (%) and effect of various substituents. First we studied the effect of catalyst amount on reaction time and conversion (%) to the desired product. We performed the reaction by varying catalyst amount from 5 to 20 mg. Table 5B.4 shows the effect of catalyst amount on conversion (%) for nitro-aldol condensation reaction over LDH3 (O).

An increase in percentage conversion from 95 to 97% is observed on increasing the amount of catalyst from 5 to 10 mg. The time required to complete the reaction also becomes gradually decreases from 10 to 7 min (entries 1–2). However, on increasing the amount upto 20 mg, the reaction time is again decreases to 4 min but, no major differences in the % conversion was observed (entries 3–4). The active basic sites of the catalyst may get saturated and agglomerated over higher dosage, resulting in the lower conversion even at higher catalyst amount. Therefore, we have selected the 5 mg as the optimum catalyst amount for further investigations.

Table 5B.4. Effect of catalyst amount on conversion (%) of nitro-aldol condensation reaction over LDH3 (O)^a.

Entry	Catalyst (mg)	Time(min)	Conversion (%) ^b
1	5	10	95
2	10	7	97
3	15	6	97
4	20	4	98

^a Reaction conditions: 1 mmol 4-nitrobenzaldehyde, 10 mmol nitromethane, 40% MW power (280 Watt), Temperature 50 °C. ^b Determined from ¹H NMR data of crude mixture.

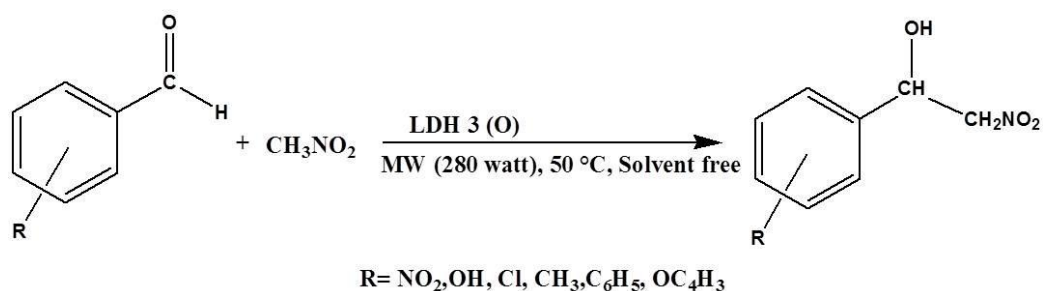
We have also studied the effect of MW power on the reaction time as well as on conversion (%) and the results are presented in Table 5B.5. For these purpose, we varied the MW power (%) from 30% (210 watt) to 50% (350 watt). It is observed that on increasing the power from 30 to 40%, the time required for completing the reaction decreases from 10 to 7 min. At the same time, the conversion (%) gets increased from 94 to 97% (entries 1–3). Again, on increasing the power upto 50%, the time required become decreases to 5 min and conversion (%) become 98% (entries 4). Thus, although the reaction time decreases on increasing the MW power to 50%, the conversion is almost similar. Therefore, we have preferred 40% MW power (280 Watt) as optimum power using 10 mg of catalyst under the solvent free MW condition.

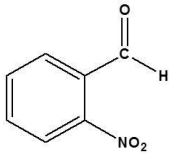
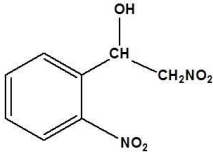
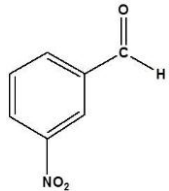
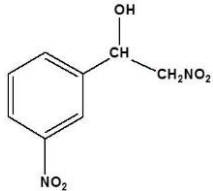
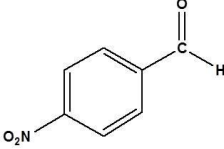
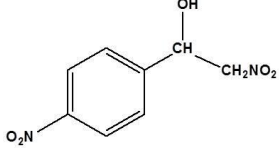
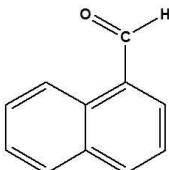
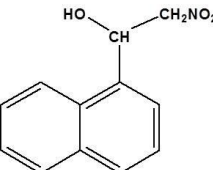
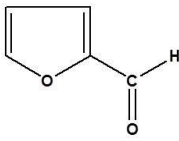
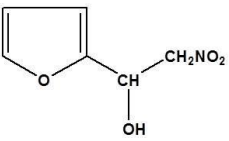
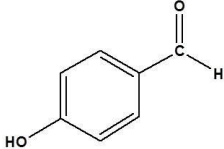
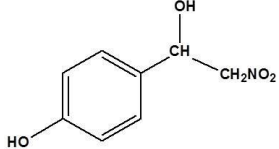
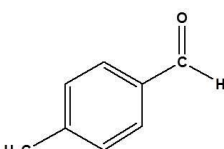
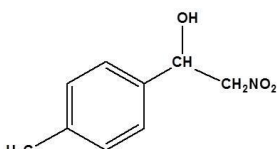
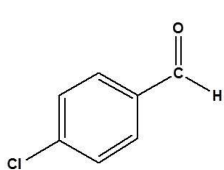
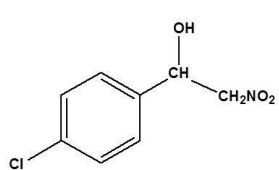
Table 5B.5. Effect of MW power (%) on conversion (%) of nitro-aldol condensation reaction over LDH3 (O)^a.

Entry	Power (%)	Time(min)	Conversion (%) ^b
1	30 (210 watt)	10	94
2	35 (245 watt)	9	95
3	40 (280 watt)	7	97
4	50 (350 watt)	5	98

^aReaction conditions: 1mmol 4-nitrobenzaldehyde, 10 mmol nitromethane, 10 mg catalyst, Temperature 50 °C. ^bDetermined from ¹H NMR data of crude mixture.

After getting our optimizing conditions for the reaction, next we have carried out the reaction with different aldehydes to observe the effect of various substituents on conversion (%). The reaction was employed with a variety of aldehydes, such as aldehydes with substrates bearing electron withdrawing groups, electron donating groups and polycyclic aromatic aldehydes. Table 5B.6 shows that conversions (%) as well as the reaction time have been greatly affected by types of substituent. The substrates bearing electron withdrawing groups (entries 1–3) give higher conversion (%) from 95 to 97% in less time (7–12 min) compared to that of the other substrates. A maximum of 30 min reaction time was considered for comparison. The substrates bearing electron donating groups exhibit % conversion of 80–88% (entries 6–8); while in case of polycyclic aromatic aldehydes, very less conversion of 64–70% is observed in 30 min (entries 4–5).

Table 5B.6. Nitro-aldol condensation reaction of nitromethane with different aldehydes over LDH3 (O)^a.

Entry	Aldehydes	Product	Temp. (°C)	Time (min)	Conversion (%) ^c
1			50	10	97
2			50	12	95
3			50	7	97 ^b
4			50	30	64
5			50	30	70
6			50	30	82
7			50	30	80
8			50	30	88

^aReaction conditions: 1 mmol aldehyde, 10 mmol nitromethane, 10 mg catalyst, 40% MW power (280 Watt), ^b Isolated pure product, ^c Determined from ¹H NMR data of crude mixture.

From practical point of view, it is important to carry out the recyclability test of a catalyst for their long term use with high catalytic activity. Figure 5B.5 shows the recyclability test of the catalyst, LDH3 (O) as a function of conversion (%) and reaction time. For the recyclability test, we employed the reaction by taking 10 mg of the catalyst under the similar experimental conditions upto four successive cycles. It is observed that up to the first three cycles, the reaction took 8–15 min with % conversion of 92–96%. However, on increasing the number of cycles upto 4th, a decrease in the conversion (90%) is observed and the reaction time also increases to 20 min (Figure 5B.5). This decrease in the catalytic activity is attributed to the deactivation of the active sites in the catalyst and/or mechanical loss of the catalyst during separation.

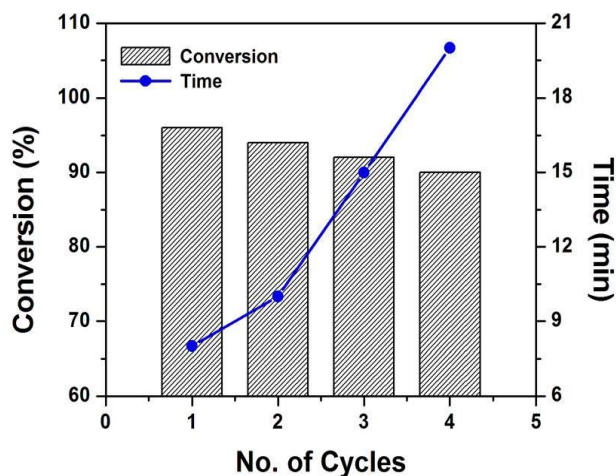
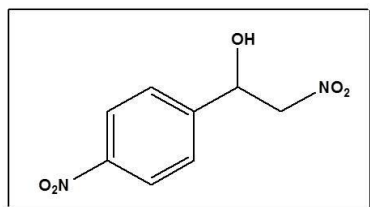


Figure 5B.5. Recyclability test of the catalyst LDH3 (O) (Reaction conditions: 1 mmol 4-nitrobenzaldehyde, 10 mmol nitromethane, 10 mg catalyst, 40% MW power (280 Watt), Temperature 50 °C).

Spectral data



2-Nitro-1-(4-nitrophenyl) ethan-1-ol)

¹H NMR (400 MHz, CDCl₃): δ 8.24-8.26 (d, $J_{\text{HH}} = 8$ Hz, 2H), 7.63-7.65 (d, $J_{\text{HH}} = 8$ Hz, 2H), 5.62 (m, 1H), 4.61 (m, 2H), 3.63 (s, 1 H); ¹³C NMR (100 MHz CDCl₃): δ 148.2, 145.4, 127.2, 124.2, 80.8, 77.1.

The ¹H and ¹³C NMR spectra of 2-Nitro-1-(4-nitrophenyl) ethan-1-ol are shown in Image A.3 and A.4 of Appendix.

In summary, we have synthesized a series of NiMgAl LDHs with varying molar ratio of divalent metal cations ($\text{Ni}^{2+}/\text{Mg}^{2+}$) by using simple co-precipitation method followed by calcination at 450 °C for 6h. The PXRD patterns reveal the formation of layered structure with secondary crystalline phases on substitution of Ni^{2+} ion in MgAl LDH. The formation of mixed oxides has been confirmed by the absence of characteristic peaks that corresponding to LDH materials. The catalytic measurements of the derived mixed oxides have been evaluated for nitro-aldol condensation reaction under solvent free MW condition. The molar ratio of divalent cations ($\text{Ni}^{2+}/\text{Mg}^{2+}$) greatly influences the % conversion of the reaction. The LDH3 (O) mixed oxide with $\text{Ni}^{2+}/\text{Mg}^{2+} = 1$, shows superior catalytic activity towards nitro-aldol condensation reaction with 97% conversion in 7 min. The enhanced activity of the catalyst, LDH3 (O) is ascribed due to the presence of equivalent amount of divalent metal cations ($\text{Ni}^{2+}/\text{Mg}^{2+} = 1$), resulting high BET surface area of 753 m^2/g with pore volume 1.28 cm^3/g . The catalyst amount and MW power (%) show great impact on the reaction time, but not much on the % conversion. The reusability test shows that the catalyst can be reused upto 4 cycles without any significant loss in catalytic efficiency.

REFERENCES

- [1] Choudary, B. M., Ranganath, K. V. S., Pal, U., Kantam, M. L., and Sreedhar, B. Nanocrystalline MgO for asymmetric Henry and Michael reactions. *Journal of the American Chemical Society*, 127(38):13167–13171, 2005.
- [2] Palomo, C., Oiarbide, M., and Laso, A. Recent advances in the catalytic asymmetric nitroaldol (Henry) reaction. *European Journal of Organic Chemistry*, 2007(16):2561–2574, 2007.
- [3] Devi, R., Borah, R., and Deka, R. C., Design of zeolite catalysts for nitroaldol reaction under mild condition. *Applied Catalysis A: General*, 433–434(8):122–127, 2012.
- [4] Blay, G., Hernández-Olmos, V., and Pedro, J. R. A catalytic highly enantioselective direct synthesis of 2-bromo-2-nitroalkan-1-ols through a Henry reaction. *Chemical Communications*, 4840–4842, 2008.
- [5] Choudary, B. M., Kavita, B., Sreenivasa Chowdari, N., Sreedhar, B., and Kantam, M. L. Layered double hydroxides containing chiral organic guests : Synthesis, characterization and application for assymmetric C–C bond forming reactions. *Catalysis Letters*, 78(1):373–377, 2002.
- [6] Majhi, A., Kadam, S. T., and Kim, S. S. TMEDA catalyzed Henry (nitroaldol) reaction under metal and solvent-free conditions. *Bulletin of the Korean Chemical Society*, 30(8):1767–1770, 2009.
- [7] Choudary, B. M., Kantam, M. L., Reddy, Ch. V., Rao, K. K., and Figueras, F. Henry reactions catalysed by modified Mg–Al hydrotalcite: An efficient reusable solid base for selective synthesis of b-nitroalkanols. *Green Chemistry*, 1(4):187–189, 1999.
- [8] Varma, R. S., Dahiya, R., and Kumar, S. Microwave-assisted Henry reaction: Solventless synthesis of conjugated nitroalkenes. *Tetrahedron Letters*, 38(29):5131–5134, 1997.
- [9] Marjani, K., Asgari, M., Ashouri, A., Mahdavinia, G. H., and Ahangar, H. A. Microwave-assisted aldol condensation of benzil with ketones. *Chinese Chemical Letters*, 20(4):401–403, 2009.

- [10] Fan, G., Li, F., Evans, D. G., and Duan, X. Catalytic applications of layered double hydroxides: Recent advances and perspectives. *Chemical Society Reviews*, 43(20):7040-7066, 2014.
- [11] Miyata, S. Anion-exchange properties of hydrotalcite-like compounds. *Clays and Clay Minerals*, 31(4):305–311, 1983.
- [12] Feng, J., He, Y., Liu, Y., Du, Y., and Li, D. Supported catalysts based on layered double hydroxides for catalytic oxidation and hydrogenation: General functionality and promising application prospects. *Chemical Society Reviews*, 44(15):5291–5319, 2015.
- [13] Liu, J. and Zhang, G. Recent advances in synthesis and applications of clay-based photocatalysts: A review. *Physical Chemistry Chemical Physics*, 16(18):8178–8192, 2014.
- [14] Marcu, I. -C., Tanchoux, N., Fajula, F., and Tichit, D. Catalytic conversion of ethanol into butanol over M–Mg–Al mixed oxide catalysts (M = Pd, Ag, Mn, Fe, Cu, Sm, Yb) obtained from LDH precursors. *Catalysis Letters*, 143(1):23–30, 2013.
- [15] Du, X., Zhang, D., Gao, R., Huang, L., Shi, L., and Zhang, J. Design of modular catalysts derived from NiMgAl-LDH@m-SiO₂ with dual confinement effects for dry reforming of methane. *Chemical Communications*, 49(60):6770–6772, 2013.
- [16] Li, H., Zhang, D., Maitarad, P., Shi, L., Gao, R., Zhang, J., and Cao, W. In situ synthesis of 3D flower-like NiMnFe mixed oxides as monolith catalysts for selective catalytic reduction of NO with NH₃. *Chemical Communications*, 48(86):10645–10647, 2012.
- [17] Lu, Z., Qian, L., Tian, Y., Li, Y., Sun, X., and Duan, X. Ternary NiFeMn layered double hydroxides as highly-efficient oxygen evolution catalysts. *Chemical Communications*, 52(5):908–911, 2016.
- [18] Trakarnpruk, W. Preparation and catalytic property of high surface area mixed oxides from calcination of MgCuCr- and MgCuAl-layered double hydroxides. *Journal of Metals Materials and Minerals*, 22(2):131–136, 2012.
- [19] Parida, K., Mohapatra, L., and Baliaarsingh, N. Effect of Co²⁺ substitution in the framework of carbonate intercalated Cu/Cr LDH on structural, electronic, optical,

- and photocatalytic properties. *The Journal of Physical Chemistry C*, 116(42):22417–22424, 2012.
- [20] Pérez, C. N., Pérez, C. A., Henriques, C. A., and Monteiro, J. L. F. Hydrotalcites as precursors for Mg, Al-mixed oxides used as catalysts on the aldol condensation of citral with acetone. *Applied Catalysis A: General*, 272 (1–2):229–240, 2004.
- [21] Zhang, M., Zhao, Y., Liu, Q., Yang, L., Fan, G., and Li, F. A La-doped Mg–Al mixed metal oxide supported copper catalyst with enhanced catalytic performance in transfer dehydrogenation of 1-decanol. *Dalton Transactions*, 45:1093–1102, 2016.
- [22] Xie, R., Fan, G., Yang, L., and Li, F. Solvent-free oxidation of ethylbenzene over hierarchical flower-like core–shell structured Co-based mixed metal oxides with significantly enhanced catalytic performance. *Catalysis Science & Technology*, 5:540–548, 2015.
- [23] Gao, W., Li, C., Chen, H., Wu, M., He, S., Wei, M., Evans, D. G., and Duan, X. Supported nickel–iron nanocomposites as a bifunctional catalyst towards hydrogen generation from $\text{N}_2\text{H}_4 \cdot \text{H}_2\text{O}$. *Green Chemistry*, 16:1560–1568, 2014.
- [24] Bharali, D., Devi, R., Bharali, P., and Deka, R. C. Synthesis of high surface area mixed metal oxide from the NiMgAl LDH precursor for nitro-aldol condensation reaction. *New Journal of Chemistry*, 39:172–178, 2015.
- [25] Labidi, N. N., Ghorbel, A., Tichit, D., and Delahay, G. Catalytic activity of CoMgAl, CoAl and MgAl of mixed oxides derived from hydrotalcites in the selective catalytic reduction of NO with ammonia. *Reaction Kinetics and Catalysis Letters*, 88(2):261–268, 2006.
- [26] Gawande, M. B., Pandey, R. K., and Jayaram, R. V. Role of mixed metal oxides in catalysis science—versatile applications in organic synthesis. *Catalysis Science & Technology*, 2(6):1113–1125, 2012.
- [27] Tian, Z., Li, Q., Hou, J., Pei, L., Li, Y., and Ai, S. Platinum nanocrystals supported on CoAl mixed metal oxide nanosheets derived from layered double hydroxides as catalysts for selective hydrogenation of cinnamaldehyde. *Journal of Catalysis*, 331:193–202, 2015.

- [28] Yuan, C., Wu, H. B., Xie, Y., and Lou, X. W. Mixed transition-metal oxides: Design, synthesis, and energy-related applications. *Angewandte Chemie International Edition*, 53(6):1488–1504, 2014.
- [29] Velu, S., Suzuki, K., and Gopinath, C. S. Photoemission and in situ XRD investigations on CuCoZnAl-mixed metal oxide catalysts for the oxidative steam reforming of methanol. *The Journal of Physical Chemistry B*, 106(49):12737–12746, 2002.
- [30] Zhou, S., Qian, Z., Sun, T., Xu, J., and Xia, C. Catalytic wet peroxide oxidation of phenol over Cu–Ni–Al hydrotalcite. *Applied Clay Science*, 53(4):627–633, 2011.
- [31] Velu, S., Suzuki, K., Hashimoto, S., Satoh, N., Ohashi, F., and Tomura, S. The effect of cobalt on the structural properties and reducibility of CuCoZnAl layered double hydroxides and their thermally derived mixed oxides. *Journal of Materials Chemistry*, 11:2049–2060, 2001.
- [32] Das, N. N. and Srivastava, S. C. Catalytic characterization of bi-functional catalysts derived from Pd–Mg–Al layered double hydroxides. *Bulletin of Materials Science*, 25(4):283–289, 2002.
- [33] Cavani, F., Trifiro, F., and Vaccari, A. Hydrotalcite-type anionic clays: Preparation, properties and applications. *Catalysis Today*, 11(2):173–301, 1991.
- [34] Mandal, S., Tichit, D., Lerner, D. A., Marcotte, N. Azoic dye hosted in layered double hydroxide: Physicochemical characterization of the intercalated materials. *Langmuir*, 25(18):10980–10986, 2009.
- [35] Naik, B., Hazra, S., Prasad, V. S., and Ghosh, N. N. Synthesis of Ag nanoparticles within the pores of SBA-15: An efficient catalyst for reduction of 4-nitrophenol. *Catalysis Communications*, 12(12):1104–1108, 2011.
- [36] Li, F., Jiang, X., Evans, D. G., and Duan, X. Structure and basicity of mesoporous materials from Mg/Al/In layered double hydroxides prepared by separate nucleation and aging steps method. *Journal of Porous Materials*, 12(1):55–63, 2005.

- [37] An, M., Cui, J., and Wang, L. Magnetic recyclable nanocomposite catalysts with good dispersibility and high catalytic activity. *The Journal of Physical Chemistry C*, 118(6):3062–3068, 2014.
- [38] Cwik, A., Fuchs, A., Hell, Z., and Clacens, J. -M. Nitroaldol-reaction of aldehydes in the presence of non-activated Mg:Al 2:1 hydrotalcite; a possible new mechanism for the formation of 2-aryl-1,3-dinitropropanes. *Tetrahedron*, 61(16):4015–4018, 2005.
- [39] Manikandan, R., Anitha, P., Prakash, G., Vijayan, P., and Viswanathamurthi, P. Synthesis, spectral characterization and crystal structure of Ni(II) pyridoxal thiosemicarbazone complexes and their recyclable catalytic application in the nitroaldol (Henry) reaction in ionic liquid media. *Polyhedron*, 81:619–627, 2014.
- [40] Sutradhar, M., Guedes da Silva, M. F. C., and Pombeiro, A. J. L. A new cyclic binuclear Ni(II) complex as a catalyst towards nitroaldol (Henry) reaction. *Catalysis Communications*, 57:103–106, 2014.
- [41] Constantino, V. R. L. and Pinnavaia, T. J. Basic properties of $Mg^{2+}_{1-x} Al^{3+}_x$ layered double hydroxides intercalated by carbonate, hydroxide, chloride and sulfate anions. *Inorganic Chemistry*, 34(4):883–892, 1995.
- [42] Ram Reddy, M. K., Xu, Z. P., Lu, G. Q., and Diniz da Costa, J. C. Layered double hydroxides for CO₂ capture: Structure evolution and regeneration. *Industrial & Engineering Chemistry Research*, 45(22):7504–7509, 2006.
- [43] Hutson, N. D., Speakman, S. A., and Payzant, E. A. Structural effects on the high temperature adsorption of CO₂ on a synthetic hydrotalcite. *Chemistry of Materials*, 16(21):4135–4143, 2004.
- [44] Yang, W., Kim, Y., Liu, K. T., Shahimi, M., and Tsotsis, T. T. A study by in situ techniques of the thermal evolution of the structure of a Mg–Al–CO₃ layered double hydroxide. *Chemical Engineering Science*, 57(15):2945–2953, 2002.
- [45] Tichit, D., Bennani, M. N., Figueras, F., and Ruiz, J. R. Decomposition processes and characterization of the surface basicity of Cl⁻ and CO₃²⁻ hydrotalcites. *Langmuir*, 14(8):2086–2091, 1998.

- [46] Bellotto, M., Rebours, B., Clause, O., Lynch, J., Bazin, D., and Elkaïm, E. Hydrotalcite decomposition mechanism: A clue to the structure and reactivity of spinel-like mixed oxides. *The Journal of Physical Chemistry*, 100(20):8535–8542, 1996.
- [47] Pe´rez, C. N., Monteiro, J. L. F., Nieto, J. M. L., and Henriques, C. A. Influence of basic properties of Mg,Al-mixed oxides on their catalytic activity in Knoevenagel condensation between benzaldehyde and phenylsulfonylacetonitrile. *Química Nova*, 32(9):2341–2346, 2009.
- [48] Corma, A., Iborra, S., Primo, J., and Rey, F. One-step synthesis of citrionitril on hydrotalcite derived base catalysts. *Applied Catalysis A: General*, 114(2):215–225, 1994.
- [49] Climent, M. J., Corma, A., Iborra, S., and Primo, J. Base catalysis for fine chemicals production: Claisen-Schmidt condensation on zeolites and hydrotalcites for the production of chalcones and flavanones of pharmaceutical interest. *Journal of Catalysis*, 151(1):60–66, 1995.
- [50] Climent, M. J., Corma, A., Iborra, S., Epping, K., and Velty, A. Increasing the basicity and catalytic activity of hydrotalcites by different synthesis procedures. *Journal of Catalysis*, 225(2):316–326, 2004.
- [51] Di Cosimo, J. I., Díez, V. K., Xu, M., Iglesias, E., and Apestegía, C. R. Structure and surface and catalytic properties of Mg-Al basic oxides. *Journal of Catalysis*, 178(2):499–510, 1998.
- [52] Baliarsingh, N., Parida, K. M., and Pradhan, G. C. Effects of Co, Ni, Cu, and Zn on photophysical and photocatalytic properties of carbonate intercalated M^{II}/Cr LDHs for enhanced photodegradation of methyl orange. *Industrial & Engineering Chemistry Research*, 53(10):3834–3841, 2014.
- [53] Klemkaite, K., Prosycevas, I., Taraskevicius, R., Khinsky, A., and Kareiva, A. Synthesis and characterization of layered double hydroxides with different cations (Mg, Co, Ni, Al), decomposition and reformation of mixed metal oxides to layered structures. *Central European Journal of Chemistry*, 9(2):275–282, 2011.